28. Schmucker-Weidelt-Kolloquium fur Elektromagnetische Tiefenforschung, 23.-27. September 2019 in Haltern am See

Prospectus for TEM Source-Oriented Imaging Using Drone-Based Data Acquisition

Bryan James[1]
[1] Consulting and Research Geophysicist, Lakewood, Colorado, USA

Introduction

- Drone-based electromagnetic (EM) sensing for semi-airborne surveys [1] promises higher data quality, better geoelectric structure resolution, and lower cost compared to ground or typical (semi-)airborne techniques, especially in terms of providing very high spatial data density
- "Source-oriented analysis" (SOA) of such densely sampled transient EM (TEM) data is proposed to estimate the induced current distributions in the presence of geoelectric structures to obtain high resolution resistivity images of the subsurface
- SOA promises to be a more intuitive, effective approach to resolve subsurface geoelectric structure compared to "field-oriented modeling" techniques including 1D and 3D inversions
- Early work on TEM SOA occurred in the 80s and early 90s [2-5], when it was determined that the approach was ill-suited for data acquisition capabilities of that time as well as being too expensive
- Recent advent of high data density drone-based EM acquisition systems [6,7] and their much lower cost compared to ground or aircraft surveys, means it is time to revisit the TEM SOA subject

Study Goals

- Describe source-oriented analysis approach as applied to TEM exploration
- Model study of multiple large loop sources on ground surface and drone-based magnetic field data acquisition system flying a few meters above the ground surface for a buried basin target structure
- Establish efficacy of the source-oriented analysis approach
- Indicate prospects for further development and capabilities

Source-Oriented TEM Methodology

TEM SOA is inspired by gravity and magnetics analysis, where the static fields are uncoupled, and the method (adding/subtracting mass or magnetization incrementally) is very simple. In TEM, however, the fields are coupled both spatially and temporally. Therefore creating and modifying timeslices of current distributions (the sources of the measured magnetic fields) cannot be done freely. So TEM SOA begins with calculation of both magnetic and subsurface electric fields for a starting model, which is then modified. Development to date shows it is best to use a simple uniform halfspace (HS) as the starting model. The point of TEM SOA is to track interaction of the current distribution evolution with the subsurface geoelectric structure. Note that any subsurface structure is illuminated by a single source's current distribution diffusion in a particular way that varies in sensitivity to specific structural elements. So TEM SOA uses multiple sources to provide different diffusing current distribution interactions with the structural elements, thus improving overall sensitivity and resolution. Sources on both sides of the target area are recommended. Figure 1 shows the simulated test model, survey layout, and a sketch of multi-source current evolution. Figure 2 shows the overall TEM SOA processing flow chart.

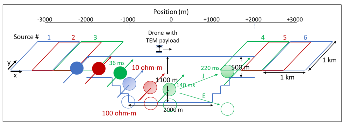

Fig. 1. Schematic of simulated buried basin test model and survey layout. Overlaid is a sketch of the left-to-right diffusion of the main peak of the current distributions from sources on the left side of the structure into the buried basin structure. Solid circles show peak current locations at 36 ms; shaded circles show future times. Empty circles depict locations of electric field. Right side sources similar, not shown.

1. Modeling Preliminaries
a) define reference model
b) perform H & E calculations for reference models

→

2. Imaging Preliminaries
a) input collected H data and calculated H & E fields for reference model
b) calculate geometric factors for Biot-Savart calculations
c) calculate significance masks as f(t,timeslice)

→

3. Optimize current distributions for all time slices and sources:
a) basic time-slip adjustments (H_x)
b) final adjustments using H_x & H_t residuals

→

4. Form Image
a) integrate adjusted current distributions over time, element by element, *using significance mask*
b) similar integration for reference current distributions
c) use [reference/adjusted] ratio to adjust resistivity of elements up or down to produce image resistivity section.

Fig. 2. TEM SOA flow chart. See text for explanations.

Figure 3 shows the reference model data for a single time slice of data for one loop source; the magnetic field profiles (H_x, H_z and H_{tot}) and the cross section of current density (J_y) are perpendicular to the simulated basin structure such that we are solving a two-dimensional (2D) problem. (3D is in the future.) The H_x profile is well behaved and relates straightforwardly to the current distribution; the position of the H_x profile maximum closely corresponds to the lateral position of the current maximum in the earth. So the initial step focuses on the H_x data alone.

The first adjustment step finds a time slice of the starting model – likely an interpolation between two time slices – that matches the position of the maximum in the H_x field data. This is called a time slip. There are several ways to define an error model for this adjustment. Though widely used, least squares error (LS) is not the best for this; instead correlation (Corr) does the best [1-Corr]. Once a correct H_x maximum is found, an amplitude adjustment is done separately that minimizes LS. Doing adjustments from an accurate starting model maintains spatial and temporal coupling integrity of TEM fields to a high degree.

Figure 4 shows the corrected time slice of data relating to the starting case shown in Figure 3; it also reflects a resistivity vs. depth function estimated from the sequence of time slips. It turns out this first adjustment step does most of the work for purposes of constructing a useful subsurface resistivity image.

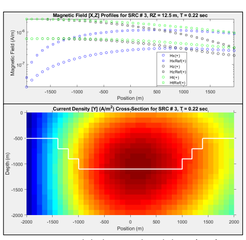

Fig. 3. Starting model plus simulated data. (Top) Magnetic field profiles (Blue: H_x, Black: H_z, Green: H_t; Circles: simulated field data, Squares: reference data) for drone-acquired data at altitude of 12.5 m. (Bottom) Current density (J_y) cross-section. Reference H data and current density calculated for 10 ohm-m uniform halfspace. Simulated model basin structure overlaid on current section in white.

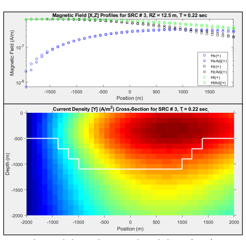

Fig. 4. Adjusted data plus simulated data. (Top) Magnetic field profiles (now Squares: adjusted data) for drone-acquired data at altitude of 12.5 m. (Bottom) Adjusted current density (J_y) cross-section. Time slice adjustment was +2.0, meaning the reference data time slice at 0.22 sec was replaced by the reference data time slice (2 time steps later) at 0.355 sec (no interpolation for whole number time slip). Amplitudes adjusted post time slip.

There are multiple possibilities for synthesizing a resistivity image from TEM SOA. The simplest is: for each subsurface element, sum the current density for the adjusted data, do the same for the reference data, ratio them $[\sum J_y^R / \sum J_y^A]$ (where superscripts R and A denote reference and adjusted, respectively), and multiply by the starting model element resistivity. However, summing over the entire time range yields an image that displays little resemblance to the modeled structure. But the current density in a given subsurface element is most closely related to its own immediate resistivity likely only during a limited duration; when the bulk of the aggregate current distribution is "far away" the current density in the element is more influenced by those other regions. Therefore a "significance mask" is created to limit the duration for summation of current density in each cell and this mask is different in each element for each source. A pair of thresholds are used for defining the significance mask bounds in each element: one relative to $J_y(t)$ and the other relative to normalized J_y(timeslice). Figure 5 shows examples of the significance mask for selected subsurface elements. It is noteworthy that in all cases the point in time where the current density in an element is at its greatest relative value in an entire current distribution time slice [J_y(timeslice)] is nearly a decade later in time than the point where it is at its maximum in time [$J_y(t)$].

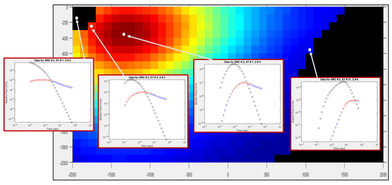

Fig. 5. An adjusted current distribution with significance mask turned on, with overlaid plots for four subsurface current elements. In the plots the black data points are the $J_y(t)$ function; the blue data points take those $J_y(t)$ values and normalize them relative to the maximum current density in each time slice, and the red data points are those included in the significance mask (data outside mask are excluded). The threshold values used to create the significance mask are .01 for the $J_y(t)$ function and .1 for the J_y(timeslice) function.

Figure 6 shows the resistivity image synthesized using the summed current ratio procedure for the simulated basin model using all 6 sources. The image agreement with the basin model is very good using just the basic current density adjustments. But recovery of resistivity values is "soft". Figure 7 shows four variations of the resistivity image for different subsets of the 6 sources (Figure 1). The version using sources 1, 3, 4, and 5 is almost as good as using all 6 and suggests the first and last in a grouping on either side of the target area are most important, much as in radio science where synthetic apertures reflect the baseline of the endpoints, being otherwise sparse. The other 3 subsets, using symmetric pairs of sources on either side of the survey area, are all deficient in matching the modeled structure, but are useful for understanding how the 6-source resistivity image is built from the 3 pairs and how sensitivity to the basin structure varies with source position. Additionally, HS starting models with resistivities of 8 and 12 ohm-m were also processed and the resistivity images formed varied only slightly from Figure 6 (for the 10 ohm-m HS starting model) and so are not shown. TEM SOA is resilient to the starting model, to a point.

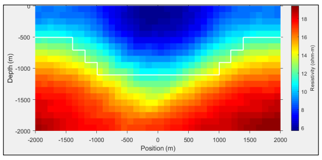

Fig. 6. Resistivity image formed using the summed current ratio procedure for 6 loop sources, 3 on each side, using the basic adjustments only (time adjustment followed by amplitude adjustment) described in the text and illustrated in Fig. 4. The summation within each pixel is limited by its significance mask as described in the text and illustrated in Fig. 5. The initial image has been smoothed once using a 9-point smoothing kernel. The modeled basin geometry is overlaid in white.

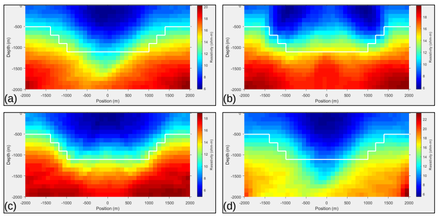

Fig. 7. Variations of resistivity image using subsets of the 6 sources modeled. (a) Using sources 1, 3, 4, and 6. (b) Using sources 1 and 6. (c) Using sources 2 and 5. (d) Using sources 3 and 4. For cases b-d, the blue regions (low resistivity) correspond to where the adjustments place excess current density, which reflects the modified paths of the highest current densities as the diffusion evolves in the presence of the structure.

Lastly we address the residuals from the misfit between corrected magnetic fields and simulated magnetic fields, as seen in Figure 4. It is now possible to use the source-oriented modeling approach used for potential fields and treat these residuals as essentially static fields. Algorithms to solve for residual current density distributions are effectively beamforming algorithms [8]. Figure 8 shows the residual current distribution from one of these algorithms and Figure 9 the updated current distribution section and magnetic field profiles once these residual results are added. A number of other similar algorithms exist in the medical imaging literature (e.g. MEG). Figure 10 shows the updated resistivity image after the residual adjustments; it shows slight changes from the Figure 6 resistivity image based only on basic adjustments.

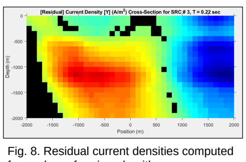

Fig. 8. Residual current densities computed from a beamforming algorithm.

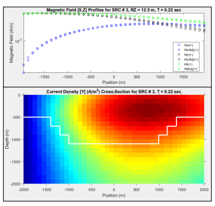

Fig. 9. Adjusted magnetic fields and current density distribution following calculation of residuals. Compare with Fig. 4 for basic-only adjustment.

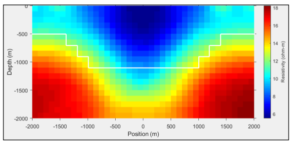

Fig. 10. Resistivity image from adjusted current densities following residual adjustments. Compare with Fig. 6 for image resulting from basic-only adjustments.

Conclusions

- TEM SOA concept is described and shown to be effective for modeled test case
- TEM SOA enabled by dense data acquisition provided by low cost drone-based systems
- Resistivity image constructed that well matches modeled buried basin structure
- Imaging result can stand alone or be used as starting point for further TEM modeling
- TEM SOA can be advanced, e.g., using differentials & further beamforming concepts

Acknowledgments: The author expresses his gratitude to Andrei Swidinsky, Johannes Stoll and Ron Bell for their numerous worthwhile discussions on TEM source-oriented analysis and their excellent, kind feedback on improvements to this poster.

Works Cited
1. Elliott, P., The Principles and practice of FLAIRTEM: Exploration Geophysics, 29(1/2), **1998**, pp. 58-60.
2. James, B.A., Detection of tunnels by transient electromagnetic subsurface imaging: U.S. Geological Survey Open-File Report 88-218, **1988**.
3. James, B.A., Transient electromagnetic imaging of a basin margin underneath the Savannah River Plant, Aiken, South Carolina: Consultant's report prepared for Westinghouse Savannah River Company, Aiken, South Carolina, **1989**.
4. Hoekstra, P., Stoyer, C.H., James, B.A., and Blohm, M.W., Characterization of reservoir rocks and fluids by surface electromagnetic transient methods: Final report prepared for U.S. DOE, Fossil Energy Section, Contract No. DE-AC22-90BC14476, Bartlesville, Oklahoma, **1992**.
5. James, B.A., and Borns, D.J., Transient electromagnetic two-dimensional subsurface resistivity imaging near the Waste Isolation Pilot Plant, Carlsbad, New Mexico: SAND report, Sandia National Laboratories, Albuquerque, New Mexico, **1993**.
6. Liu,, F., Huang, L., Lihua, L., Li, J., Geng, Z., Zhang, Q., and Fang, G., A New Semi-airborne Transient Electromagnetic System and Application of Detecting Underground Conductor in East Uminqin Banner, China: 7th Int'l Conf. Env. and Eng. Geoph & Summit Forum of Chinese Acad. of Eng. on Eng. Sci. and Tech., **2016**, pp. 420-423.
7. Stoll, J.B., Noellenburg, R., Kordes, T., Becken, M., Yogeshwar, P., Bergers, R., and Matzander, U., Semi-Airborne Electromagnetics Using a Multicopter: Extended Abstract at GEM 2019 Xi'an: Int'l Workshop on Gravity, Electrical & Magnetic Methods and Their Applications, Xi'an, China, May 19-22, **2019**.
8. Fuchs, A., Beamforming and Its Applications to Brain Connectivity, in: Jirsa, V.K., and McIntosh, A., (eds) Handbook of Brain Connectivity. Understanding Complex Systems. Springer, Berlin, Heidelberg. **2007**, pp. 357-378.